

Published in final edited form as:

Sci Signal. ; 7(318): ra29. doi:10.1126/scisignal.2005125.

Antagonism of EGFR and HER3 Enhances the Response to Inhibitors of the PI3K-Akt Pathway in Triple-Negative Breast Cancer

Jessica J. Tao^{1,*}, Pau Castel^{2,*}, Nina Radosevic-Robin^{3,4,*}, Moshe Elkabets², Neil Auricchio¹, Nicola Aceto¹, Gregory Weitsman⁵, Paul Barber^{6,7}, Borivoj Vojnovic^{6,8}, Haley Ellis², Natasha Morse², Nerissa Therese Viola-Villegas⁹, Ana Bosch², Dejan Juric¹, Saswati Hazra¹⁰, Sharat Singh¹⁰, Phillip Kim¹⁰, Anna Bergamaschi¹¹, Shyamala Maheswaran¹, Tony Ng^{5,12}, Frédérique Penault-Llorca^{3,4}, Jason S. Lewis⁹, Lisa A. Carey¹³, Charles M. Perou¹⁴, José Baselga^{2,†}, and Maurizio Scaltriti^{2,†}

¹Massachusetts General Hospital Cancer Center and Harvard Medical School, 149 13th Street, Charlestown, MA 02129, USA

²Human Oncology & Pathogenesis Program, Memorial Sloan Kettering Cancer Center, 1275 York Avenue, Box 20, New York, NY 10065, USA

³Department of Biopathology, Centre Jean Perrin, 58 rue Montalembert, 63011 Clermont-Ferrand, France

⁴ERTICA EA4677, University of Auvergne, 63000 Clermont-Ferrand, France

⁵Richard Dumbleby Department of Cancer Research, Randall Division of Cell & Molecular Biophysics and Division of Cancer Studies, King's College London, London SE1 1UL, UK

⁶Gray Institute for Radiation Oncology and Biology, Department of Oncology, University of Oxford, Old Road Campus Research Building, Roosevelt Drive, Oxford OX3 7DQ, UK

⁷Institute for Mathematical and Molecular Bio-medicine, King's College London, London SE1 1UL, UK

⁸Randall Division of Cell & Molecular Biophysics, King's College London, London SE1 1UL, UK

⁹Department of Radiology and Program in Molecular Pharmacology and Chemistry, Memorial Sloan Kettering Cancer Center, New York, NY 10065, USA

†Corresponding author: scaltrim@mskcc.org (M.S.); baselgaj@mskcc.org (J.B.).

*These authors contributed equally to this work.

Author contributions: J.J.T., P.C., D.J., J.B., and M.S. designed the research. J.J.T., P.C., N. Auricchio, M.E., A. Bosch, H.E., N.M., and N. Aceto performed the experiments. N.R.-R. and F.P.-L. collected and analyzed the human specimens. S.H., S.S., and P.K. performed the CEER arrays and their analyses. S.M. assisted with the design of the research. G.W., P.B., B.V., and T.N. performed and analyzed the FRET experiments on patient samples. L.A.C. and C.M.P. provided the gene expression data, which were analyzed by A. Bergamaschi, J.S.L., and N.T.V.-V. A. Bergamaschi, J.S.L., and N.T.V.-V. produced and analyzed the in vivo imaging data. N.R.-R., J.J.T., and M.E. prepared the figures and analyzed the cellular and in vivo data. J.J.T., J.B., and M.S. wrote the manuscript.

Competing interests: S.H., S.S., and P.K. are employees of Prometheus Therapeutics & Diagnostics. M.S. is a consultant for Prometheus Therapeutics & Diagnostics. J.B. had consultant and advisory roles at Genentech. C.M.P. is an equity stock holder and a member of the Board of Directors of BioClassifier LLC and University Genomics.

Supplementary Materials: www.sciencesignaling.org/cgi/content/full/7/318/ra29/DC1

¹⁰Prometheus Therapeutics & Diagnostics, 9410 Carroll Park Drive, San Diego, CA 92121, USA

¹¹Department of Molecular and Integrative Physiology, University of Illinois at Urbana-Champaign, 524 Burrill Hall, 407 South Goodwin Avenue, Urbana, IL 61801, USA

¹²UCL Cancer Institute, Paul O'Gorman Building, University College London, London WC1E 6DD, UK

¹³Department of Medicine, University of North Carolina at Chapel Hill, 170 Manning Drive, Chapel Hill, NC 27599, USA

¹⁴Department of Genetics, Lineberger Comprehensive Cancer Center, University of North Carolina at Chapel Hill, Chapel Hill, NC 27599, USA

Abstract

Both abundant epidermal growth factor receptor (EGFR or ErbB1) and high activity of the phosphatidylinositol 3-kinase (PI3K)–Akt pathway are common and therapeutically targeted in triple-negative breast cancer (TNBC). However, activation of another EGFR family member [human epidermal growth factor receptor 3 (HER3) (or ErbB3)] may limit the antitumor effects of these drugs. We found that TNBC cell lines cultured with the EGFR or HER3 ligand EGF or heregulin, respectively, and treated with either an Akt inhibitor (GDC-0068) or a PI3K inhibitor (GDC-0941) had increased abundance and phosphorylation of HER3. The phosphorylation of HER3 and EGFR in response to these treatments was reduced by the addition of a dual EGFR and HER3 inhibitor (MEHD7945A). MEHD7945A also decreased the phosphorylation (and activation) of EGFR and HER3 and the phosphorylation of downstream targets that occurred in response to the combination of EGFR ligands and PI3K–Akt pathway inhibitors. In culture, inhibition of the PI3K–Akt pathway combined with either MEHD7945A or knockdown of HER3 decreased cell proliferation compared with inhibition of the PI3K–Akt pathway alone. Combining either GDC-0068 or GDC-0941 with MEHD7945A inhibited the growth of xenografts derived from TNBC cell lines or from TNBC patient tumors, and this combination treatment was also more effective than combining either GDC-0068 or GDC-0941 with cetuximab, an EGFR-targeted antibody. After therapy with EGFR-targeted antibodies, some patients had residual tumors with increased HER3 abundance and EGFR/HER3 dimerization (an activating interaction). Thus, we propose that concomitant blockade of EGFR, HER3, and the PI3K–Akt pathway in TNBC should be investigated in the clinical setting.

Introduction

Triple-negative breast cancer (TNBC) is clinically defined by the absence of estrogen receptor (ER), progesterone receptor, and human epidermal growth factor receptor (EGFR) 2 (HER2) overexpression or amplification. It represents 15 to 20% of newly diagnosed breast cancer, affects women in the reproductive age, and often follows an aggressive clinical course, with early recurrences in the form of distant visceral metastases, including to the brain (1–3). On the other hand, this tumor type has been demonstrated to be more responsive to cytotoxic therapy than ER-positive breast cancers (4–6). The current neoadjuvant strategies for TNBC use taxane/ anthracycline-based regimens, which reportedly achieve “pathological complete response” (pCR; defined as no invasive and no in

situ residual tumors in breast and nodes) in about 20% of patients in unselected cohorts (7). TNBC has been described as having a high frequency of inactivation or decreased expression of the gene encoding phosphatase and tensin homolog deleted on chromosome 10 (PTEN) (1, 8), as well as overexpression of the gene encoding human EGFR in up to about 50% of cases (9, 10). These biochemical features offer the opportunity to explore novel potential therapeutic strategies in this breast cancer subtype. Clinical benefits from the EGFR inhibitor cetuximab (11, 12) and the pan-phosphatidylinositol 3-kinase (PI3K) inhibitor NVP-BKM120 (13) have been reported in TNBC patients. However, none of these studies showed durable responses.

Preclinical evidence suggests that inhibition of the PI3K-Akt-mTOR (mammalian target of rapamycin) axis induces compensatory genetic expression and activation of upstream receptor tyrosine kinases (RTKs), including EGFR and, most prominently, HER3 (also known as ErbB3) (14–17). This may reduce the antitumor effects of single-agent PI3K pathway blockade. Furthermore, studies using cellular models of cetuximab resistance suggest that HER3 itself can limit the sensitivity to cetuximab by increasing EGFR-HER3 heterodimerization and activation of downstream pathways (18). Although HER3 targeting is being explored in other breast cancer subtypes (19, 20), no rationale has yet been provided for the inhibition of this RTK in TNBC. Here, we hypothesized that targeting both EGFR and HER3 in combination with inhibition of the PI3K-Akt pathway would enhance the therapeutic response in EGFR-positive TNBC.

Results

Blockade of EGFR and HER3 combined with inhibition of the PI3K-Akt pathway results in superior antitumor activity

HCC70 and MDA-MB-468 TNBC cell lines, characterized by increased abundance of EGFR and loss of *PTEN* expression (fig. S1), were treated with GDC-0068 [a selective inhibitor of the Akt1, 2, and 3 isoforms (21)], GDC-0941 [a class I selective pan-PI3K inhibitor (22)], MEHD7945A [an antibody targeting both EGFR and HER3 (23)], or a combination of these inhibitors in the presence of either EGF or heregulin (NRG1), ligands for EGFR and HER3, respectively. Consistent with other reports (14–16), treatment with either GDC-0068 or GDC-0941 increased the abundance of HER3 and, in HCC70 cells, induced the phosphorylation (activation) of both EGFR and HER3 (Fig. 1A). The addition of MEHD7945A prevented the EGF- or NRG1-induced activation of EGFR and HER3 and reduced the phosphorylation of the downstream mTOR effector ribosomal protein S6 and extracellular signal-regulated kinase (ERK) pathways in both cell lines (Fig. 1A). The effects of MEHD7945A on the phosphorylation of ERK in cells triggered by EGF are mild, likely because of the high abundance of EGFR in these cells. Notably, GDC-0068 competes for the adenosine 5'-triphosphate (ATP)-binding site of Akt and is known to cause increased phosphorylation of the enzyme at its two regulatory sites [Thr³⁰⁸ and Ser⁴⁷³ (21)], as is evident in the blots.

Given its effects on Akt and ERK activation, we tested whether combining MEHD7945A with either GDC-0068 or GDC-0941 would enhance the antiproliferative response in HCC70 and MDA-MB-468 cells. In cells treated with single or double agents for 5 days, we

observed varying sensitivity to the single agents GDC-0068 and GDC-0941, but in every case, the combination of the PI3K- or Akt-targeted agents and MEHD7945A considerably inhibited cell proliferation more effectively than did either single agent (Fig. 1B).

To expand our findings *in vivo*, we first tested the efficacy of MEHD7945A in combination with either GDC-0068 or GDC-0941 in both HCC70- and MDA-MB-468–derived xenografts (fig. S2). Whereas both types of tumors responded only modestly to any of the single agents (GDC-0068, GDC-0941, or MEHD7945A), the combination of GDC-0068 or GDC-0941 and MEHD7945A yielded significantly superior tumor growth inhibition compared to monotherapy. Moreover, one-third of the animals in the cohorts of both combination regimens achieved complete tumor shrinkage, with no relapses observed 90 days after treatment cessation. We next investigated the abundance and activation of EGFR and HER3 in HCC70-derived xenografts collected at the end of each experiment. The technical challenge of obtaining reliable detection of phosphorylated HER3 by immunohistochemistry (IHC) and the small amount of tissue available from the tumors treated with the combination regimens prompted us to assess these using an alternative methodology. Frozen tissue was analyzed by collaborative enzyme enhanced reactive-immunoassay (CEER), a platform that uses reversed-phase detection of nanogram quantities of protein (22). Treatment with GDC-0068 or GDC-0941 increased the abundance and phosphorylation of both EGFR and HER3 (fig. S3 and table S1A). The increased phosphorylation of EGFR after GDC-0068 treatment was most likely a result of increased EGFR/HER3 heterodimerization because we observed no changes in the total abundance of EGFR. As expected, the cotreatment of MEH-D7945A prevented receptor phosphorylation induced by either GDC-0068 or GDC-0941.

To test the response to these treatments in patient-derived xenografts (PDXs) of TNBC, we used available patient tumors in our laboratory. These tumors were characterized by IHC to have undetectable abundance of PTEN, high abundance of EGFR, and generally high (more than 50%) staining for the proliferation marker Ki67 (fig. S4). These features predicted a particularly aggressive phenotype, confirmed by the rapid growth of the tumor xenografts in untreated mice (Fig. 1C). Single-agent treatment with GDC-0068, GDC-0941, or MEHD7945A delayed tumor growth, whereas the combination of either GDC drug with MEHD7945A caused durable tumor stasis (Fig. 1C). Consistent with the cell line–derived xenografts, the abundance of HER3 and EGFR increased after inhibition of the PI3K-Akt pathway. The addition of MEH-D7945A effectively prevented HER3 phosphorylation and kept that of EGFR at the same abundance as in control tumors (Fig. 1D and table S1B). The capability of Akt inhibitors to increase the abundance of EGFR and HER3 in PDXs was also confirmed by positron emission tomography (PET). From the PET scans, we found a visibly higher accumulation of ⁸⁹Zr-MEHD7945A in the tumor of the GDC-0068–treated cohort of mice compared to the control group (fig. S5). Quantification of the uptake of ⁸⁹Zr-MEHD7945A in GDC-0068–treated or untreated tumors revealed a nearly twofold higher tracer (⁸⁹Zr) accumulation in the treated group compared to control mice. Liver accumulation of ⁸⁹Zr-MEHD7945A is considered as the main route of excretion of the probe.

Tumor cell proliferation was also measured using the Ki67 index in specimens from xenografts collected at the experimental endpoints. We found that the percentage of Ki67-positive cells was significantly lower only in the combination therapy cohorts (fig. S6A). These results were further confirmed measuring the number of Ki67-positive circulating tumor cells (CTCs) in mice bearing PDXs greater than 1 cm³ in volume and treated for 6 days with GDC-0068, GDC-0941, MEH-D7945A, or the combination of these agents (fig. S6B). Collectively, these data show that targeting both EGFR and HER3 enhanced the antitumor effects of PI3K-Akt inhibitors.

HER3 suppression improves the antitumor activity of PI3K-Akt inhibition

To dissect the role of HER3 inhibition in these models, we compared the activity of cetuximab (an antibody targeting exclusively EGFR) with MEHD7945A, each in combination with either GDC-0068 or GDC-0941 in HCC70 cells. Both cetuximab and MEHD7945A enhanced the antiproliferative activity mediated by PI3K-Akt pathway inhibition in cells stimulated with EGF; however, MEHD7945A was more effective than cetuximab in cooperating with GDC-0068 and GDC-0941 in cells stimulated with NRG1 (Fig. 2A). The importance of specifically blocking HER3 in this setting was confirmed by testing the activity of PI3K-Akt inhibitors after HER3 knockdown by small interfering RNA (siRNA). HER3 depletion sensitized MDA-MB-468 cells to the antiproliferative activity of either GDC-0068 or GDC-0941 (fig. S7).

We next compared the antitumor effect of combining cetuximab versus MEHD7945A with GDC-0941 in HCC70-derived xenografts. Whereas the combination of cetuximab and GDC-0941 did not further inhibit tumor growth compared to either single-agent treatment, the combination of MEHD7945A and GDC-0941 (concomitantly targeting EGFR, HER3, and PI3K) was superior to either cetuximab alone or cetuximab in combination with GDC-0941 (Fig. 2B), with no palpable tumor present in four of nine cases. The combination of GDC-0068 with cetuximab (tested in both HCC70 and PDX models) appeared to inhibit tumor growth in some cases compared to either single agent, but the effect was not statistically significant (fig. S8), suggesting that adding cetuximab had no benefit over either PI3K-Akt pathway inhibitor alone. Biochemically, both MEHD7945A and cetuximab combination treatments with GDC-0941 decreased the phosphorylation of EGFR in HCC70 xenografts, but only the MEHD7945A combination decreased HER3 activation, although this was not statistically significant (Fig. 2C and table S1C). These results suggest that HER3 plays an important role in limiting the efficacy of PI3K-Akt pathway inhibitors in this model.

Decreased EGFR and increased HER3 abundance are associated with lower response to EGFR antagonists in TNBC patients

To investigate whether changes in EGFR and HER3 abundance can affect the response to anti-EGFR therapy in TNBC patients, we evaluated the abundance of these receptors in samples from patients enrolled in two pilot neoadjuvant clinical trials testing the antitumor activity of the EGFR antibodies panitumumab (47 patients) and cetuximab (29 patients) in combination with various standard chemotherapies. Of the 47 TNBC patients enrolled in the study that combined panitumumab with four standard cytotoxic agents (DNA-damaging

agents 5-fluorouracil, epirubicin, or cyclophosphamide, or the mitotic inhibitor docetaxel), 22 patients (46.8%) achieved pCR at the time of surgery (24 weeks after treatment commenced), whereas 25 patients (53.2%) showed residual disease (NCT00933517). This was a twofold increase in pCR compared to TNBC patients treated only with cytotoxic-based neoadjuvant chemotherapy (6), which underscores the benefit of adding EGFR-targeted agents in this setting. Of 29 patients enrolled in the study testing the antitumor activity of cetuximab combined with docetaxel, 8 experienced pCR (27.5%) (NCT00600249).

IHC assessment of EGFR and HER3 abundance was possible on pre-treatment samples from 16 patients who achieved pCR with panitumumab combination therapy at time of surgery and 24 patients who did not (table S2). We observed a trend toward a higher probability to achieve pCR after panitumumab treatment in patients with a pretreatment EGFR score higher than 70 (Fig. 3A). No statistical correlation was found between the pre-treatment HER3 score and the likelihood to achieve pCR in this cohort. For the cetuximab-treated patients, the analysis of EGFR and HER3 abundance before and after treatment was possible only for six of the eight patients who reached pCR; thus, because of the low sample size, we did not perform the pCR correlation analysis for the patients enrolled in the cetuximab trial. The results from the panitumumab trial at least suggest that high EGFR abundance before treatment predicts an optimal response to EGFR-targeted antibodies. However, a substantial portion (42%) of patients who had high EGFR abundance in the pretreated tumor did not show complete response; therefore, we investigated whether changes in the abundance or activity of EGFR and HER3 occurred after treatment. For patients who did not achieve pCR at the time of surgery, IHC assessment was possible on 24 and 22 paired samples for EGFR and HER3, respectively, from the panitumumab trial, and on 19 and 20 paired samples, respectively, from the cetuximab trial (table S2). When we considered only the tumors with a pretreatment EGFR score higher than 150 (12 from the panitumumab trial and 7 from the cetuximab trial), we found decreased EGFR abundance in residual tumors after treatment in 12 of 19 cases compared with that in the paired pretreatment specimens (Fig. 3, B and C). On a side note, we observed a similar trend in a different cohort of samples obtained from metastatic TNBC patients enrolled in the TBCRC 001 clinical trial (12), who were treated with cetuximab in combination with carboplatin. pCR could not be used as a parameter of response given the metastatic nature and the low response rate observed in the study, so we examined overall survival. On the basis of gene expression data from 16 paired biopsies (before and after 1 to 2 weeks of treatment), we observed decreased overall survival in patients with decreased EGFR mRNA in the posttreatment specimens (fig. S9).

The abundance of HER3 in the 22 residual (posttreatment) tumors from panitumumab-treated patients compared with their pretreatment counterparts was increased in 12 patients (Fig. 4, A and B). A similar trend was observed in cetuximab-treated patients: HER3 abundance was increased in the residual tumors of 13 of 20 available non-pCR patient samples compared with that in paired pretreatment specimens (fig. S10). When the data from both the panitumumab- and the cetuximab-treated patient samples were pooled, the increase in HER3 abundance was statistically significant (table S2). Using fluorescence resonance energy transfer (FRET) to analyze EGFR-HER3 dimerization (a mechanism of activation), we investigated whether there was increased activation in addition to increased

abundance of HER3 in the residual tumors of patients not achieving pCR from EGFR-targeted therapy. Enough tissue was available in a small cohort of specimens, three patients treated with cetuximab and four patients treated with panitumumab. Five of seven of the pooled cases displayed increased dimerization of HER3 and EGFR (Fig. 4, C and D). Together, these results suggest that increased HER3 expression and HER3 activation may mediate residual tumor growth after EGFR-targeted therapy.

Discussion

Here, we found that HER3 may play a critical role in limiting the antitumor effect of inhibitors targeting either the PI3K-Akt or EGFR pathway. We demonstrated that simultaneously targeting EGFR and HER3 by MEHD7945A enhanced the efficacy of PI3K-Akt pathway inhibitors in preclinical models of EGFR-positive TNBC. Furthermore, our clinical analysis suggests that HER3 abundance and activation are induced in TNBC patients by EGFR-targeted therapies and that this change may prevent therapy-induced tumor regression. In a study testing the clinical activity of cetuximab in TNBC, only a minority of patients whose tumors showed EGFR pathway inhibition derived clinical benefit from the therapy, suggesting that different mechanisms of receptor activation may occur in this subtype of breast cancer (12). Preclinically, low abundance of EGFR and high abundance of HER3, among others, may determine cetuximab resistance in PDX models (24). Moreover, HER3 abundance and phosphorylation (a marker of activation) are induced after Akt suppression. The first evidence of this feedback activation was reported by pioneering work from Sergina *et al.*, who also postulated that HER3 plays a pivotal role in limiting the efficacy of HER kinase inhibitors (17). These results were extensively validated using other HER inhibitors (25) or specific molecules directly targeting PI3K or Akt (14, 16). We have previously shown that this phenomenon also occurs in patients treated with the Akt inhibitor GDC-0068 (26). Therefore, our rationale behind simultaneously targeting EGFR, HER3, and PI3K in TNBC is derived from the observations that nearly half of TNBC have a high abundance of EGFR, that TNBC often has a low abundance of the endogenous Akt inhibitor PTEN, and that increased abundance and activation of HER3 appear to limit the sensitivity of TNBC to targeted therapy. It is plausible that lower doses of PI3K-Akt pathway inhibitors are required to achieve pathway suppression (and, consequently, tumor growth inhibition) when both EGFR and HER3 are inhibited. In addition, tumor cells that have a relatively high abundance of these receptors can function as molecular “flags” for immune-mediated antibody-dependent cytotoxicity, intrinsic characteristics of immunoglobulin G type I antibodies such as MEHD7945A *in vivo*. Thus, the antibody-mediated immune response may also explain, at least in part, the higher response to the drug combinations in nude mice compared to the *in vitro* setting.

In conclusion, we believe that simultaneous inhibition of EGFR, HER3, and the PI3K-Akt pathway has the potential to greatly expand the percentage of TNBC patients who can benefit from targeted therapy. Given that both pharmacokinetic and pharmacodynamic data for MEHD7945A, GDC-0068, and GDC-0941 are already available, the design of phase 2 clinical trials testing the activity of these possible combinations in TNBC would be straightforward. Patients may be enrolled on the basis of EGFR abundance in the tumors,

and HER3 abundance and activation after PI3K pathway inhibition may be measured with either biopsies collected during treatment or live imaging techniques.

Materials and Methods

Study design

The objective of our study was to test the activity of concomitant blockade of EGFR, HER3, and the PI3K-Akt pathway in preclinical models of TNBC. Moreover, we aimed to evaluate whether the expression of both EGFR and HER3 was influencing the clinical response to anti-EGFR therapy in TNBC patients. We planned to treat with GDC-0068 (Akt inhibitor), GDC-0941 (PI3K inhibitor), and MEHD7945A (antibody binding to both EGFR and HER3) TNBC cell lines and tumors to test the antitumor activity of these compounds separately and in combination. Moreover, we planned to test by IHC the expression of both EGFR and HER3 in TNBC patients who underwent cetuximab (antibody anti-EGFR)-based therapy.

In vitro experiments were performed at least two times and at least in triplicate for each replica.

Cell lines and chemical compounds

MDA-MB-468 and HCC70 were purchased from the American Type Culture Collection and maintained at 37°C in Dulbecco's modified Eagle's medium/Ham's F-12 1:1 and RPMI 1640, respectively, with 10% fetal calf serum, L-glutamine (2 mM), penicillin (20 U/ml), and streptomycin (20 µg/ml) in a humidified atmosphere and 5% CO₂. The pan-PI3K inhibitor GDC-0941 was obtained from the Stand Up To Cancer/PI3K Dream Team Mouse Pharmacy. The Akt inhibitor GDC-0068 and the dual EGFR-HER3 inhibitor MEHD7945A were provided by Genentech. All compounds were dissolved in dimethyl sulfoxide for in vitro experiments.

Cell viability and proliferation

For proliferation, 5×10^3 to 8×10^3 cells were seeded in 96-well plates and treated with the indicated concentrations of GDC-0068, GDC-0941, and/or MEHD7945A. After 5 days, cells were fixed and stained with crystal violet. Cell proliferation was also analyzed with CellTiter-Glo Luminescent Cell Viability Assay (Promega) as described by the manufacturer. For proliferation in response to heregulin (NRG1; PeproTech) and EGF (PeproTech), 5×10^4 cells were treated with GDC-0068, GDC-0941, and/or MEHD7945A in the presence of NRG1 (4 ng/ml) or EGF for 5 days and then stained with crystal violet. For siRNA experiments, 5×10^3 cells were seeded in 96-well plates and transfected with siRNA (Silencer, Ambion) control or a pool of two hairpins targeting human HER3 mRNA using DharmaFECT transfection reagent (Thermo Scientific).

Western blotting

Cells were washed with ice-cold phosphate-buffered saline (PBS) and scraped into ice-cold radioimmunoprecipitation assay lysis buffer (Cell Signaling Technology) supplemented with phosphatase inhibitor cocktails (Complete Mini and PhosphoStop, Roche). Lysates were

cleared by centrifugation at 13,000 rpm for 10 min at 4°C, and supernatants were removed and assayed for protein concentration using the Pierce BCA Protein Assay Kit (Thermo Scientific). Thirty-five micrograms of total lysate was resolved on NuPAGE 4 to 12% bis-tris gels (Life Technologies) and electrophoretically transferred to Immobilon transfer membranes (Millipore). Membranes were blocked for 1 hour in 5% nonfat dry milk in tris-buffered saline (TBS)-Tween and then hybridized using the following primary antibodies in 5% bovine serum albumin (BSA) TBS-Tween: phospho-Akt (Ser⁴⁷³), phospho-Akt (Thr³⁰⁸), Akt, phospho-S6 (Ser^{240/4}), phospho-S6 (Ser^{235/6}), S6, phospho-ERK (Thr²⁰²/Tyr²⁰⁴), ERK, phospho-EGFR (Tyr¹⁰⁶⁸), EGFR, phospho-HER3 (Tyr¹²⁸⁹), and HER3 (1:500 to 1:1000; Cell Signaling Technology). b-Actin was used as a loading control (1:5000; Sigma), also in 5% BSA TBS-Tween. Mouse and rabbit horseradish peroxidase (HRP)-conjugated secondary antibodies (1:50,000; Amersham Biosciences) were diluted in 2% nonfat dry milk in TBS-Tween. Protein-antibody complexes were detected by chemiluminescence with SuperSignal West Femto Chemiluminescent Substrate (Thermo Scientific), and images were captured with a G:BOX camera system.

Establishment of tumor xenografts and in vivo treatments

All mouse studies were conducted through Institutional Animal Care and Use Committee-approved animal protocols in accordance with institutional guidelines. Six-week-old female athymic nude mice were purchased from Charles River Laboratories and housed in air-filtered laminar flow cabinets with a 12-hour light cycle and food and water ad libitum. The size of the animal groups was calculated to measure means difference between placebo and treatment groups of 25% with a power of 80% and a *P* value of 0.01. Host mice carrying xenografts were randomly and equally assigned to either control or treatment groups. Animal experiments were conducted in a controlled and nonblinded manner. For cell line-derived xenograft studies, mice were injected subcutaneously with 1×10^7 HCC70 or MDA-MB-468 suspended in 150 μ l of culture medium/Matrigel (BD Biosciences) in a 4:1 ratio. 17 β -Estradiol (1 μ M) was supplemented in the mouse drinking water as described (27).

For PDX studies, tumors were subcutaneously implanted in 6-week-old female athymic nude mice. Upon xenograft growth, tumor tissue was reimplanted into recipient mice, which were randomized upon implant growth. For the collection of CTCs, tumors were implanted into the mammary pad of athymic nude mice.

Once tumors reached an average volume of ~ 150 to 250 mm³, mice were randomized into treatment arms, with 7 to 11 tumors per group. GDC-0068 (40 mg/kg) or GDC-0941 (75 mg/kg) was dissolved in 0.5% methylcellulose and 0.2% Tween-80 (MCT) solution and administered once daily via oral gavage. MEHD7945A (10 mg/kg) and cetuximab (10 mg/kg) were diluted in PBS and injected intraperitoneally twice weekly. Tumors were measured by digital caliper over the entire treatment period and harvested 2 hours after the last administration of the drug. Tumor volume was determined using the following formula: $(\text{length} \times \text{width}^2) \times (\pi/6)$. Tumor volumes are plotted as means \pm SEM.

Small-animal immuno-PET

Preparation of ^{89}Zr -MEHD7945A: The MEHD7945A monoclonal antibody (mAb) was functionalized with *p*-isothiocyanatobenzyl-desferrioxamine (DFO-Bz-NCS, Macrocylics Inc.) with a 1:7 mAb/DFO-Bz-NCS ratio. The reaction was incubated at 37°C for 1 hour. The modified antibodies were purified using a 10-kD centrifugal filter (GE Vivaspin 500). ^{89}Zr was produced through proton beam bombardment of yttrium foil and isolated in high purity as ^{89}Zr -oxalate at Memorial Sloan Kettering Cancer Center according to previously established procedure (28). Labeling of the MEHD7945A-DFO conjugate proceeded as described (29) with an obtained specific activity of 2.5 to 3 mCi/mg and >95% purities. PET imaging: Scans were recorded with a microPET Focus 120 (Concorde Microsystems). Mice ($n = 3$ for each group, bearing two tumors on each flank) were administered with ^{89}Zr -MEH-D7945A (150 to 200 μCi , 50 to 68 μg) in 100 μl of 0.9% saline formulations via lateral tail vein injections. Whole-body acquisitions were acquired on mice while anesthetized with 1.5 to 2.0% isoflurane (Baxter Healthcare) in oxygen at 24 to 120 hours after injection. Images were reconstructed via filtered back projection. The images were analyzed using ASIPro VM software (Concorde Microsystems). Volumes of interest (VOIs) were measured on various planar sections of the acquired image by manually drawing on the tumor site. The average VOI was calculated and expressed as percent injected dose per gram of tumor tissue (%ID/g). Data values were expressed as means \pm SD unless otherwise stated. Statistical analysis was performed with GraphPad Prism version 6.02 software using Student's *t* test. A *P* value of <0.05 is considered statistically significant.

Collaborative enzyme enhanced reactive-immunoassay

The abundance and phosphorylation of EGFR and HER3 in xenografts were determined by CEER (30, 31). CEER uses the formation of unique immunocomplexes between capture antibodies printed on a nitrocellulose microarray surface, with which the target molecule in cell lysates reacts, and two independent detector antibodies. One detector antibody is conjugated to glucose oxidase, and the other is conjugated to HRP. Target detection [expressed as computational unit (CU)] requires the presence of both detector antibodies, and the enzyme channeling event between glucose oxidase and HRP will not occur unless both antibodies are in close proximity. For each assay, a standard curve was generated from eight concentrations of serially diluted reference lysates from cell lines, well characterized for the abundance and phosphorylation of RTKs. Each assay included controls along with sample lysates. When control lysates provided acceptable values, signals generated from samples were quantified against the standard curve. One computational unit for EGFR represented about 10^6 molecules, whereas 1 CU for HER3 represented about 5×10^4 molecules. Raw data were normalized by the total amount of cytokeratins (CKs) to include only protein expressed in the epithelial compartment (table S1).

Circulating tumor cells

CTCs were captured on the herringbone chip, fixed, and permeabilized as previously described (32). For capture, the herringbone chip was coated with antibodies against EpCAM (epithelial cell adhesion molecule) (R&D Systems) and EGFR (cetuximab; Eli Lilly) (33). The CTC-containing chip was incubated with primary antibodies against wide-

spectrum CKs (Abcam), CD45 (Santa Cruz Biotechnology), and Ki67 (Life Technologies), and secondary antibodies were conjugated with Alexa Fluor 647, Alexa Fluor 555, and Alexa Fluor 488 (all from Life Technologies). Nuclei were stained with 4',6'-diamidino-2-phenylindole (DAPI). We used an automated fluorescence microscopy scanning system (BioView) to identify Ki67-positive CTCs (CK⁺/CD45⁻/Ki67⁺), Ki67-negative CTCs (CK⁺/CD45⁻/Ki67⁻), and contaminating white blood cells (CD45⁺).

Immunohistochemistry

For IHC on xenografts, dissected tissues were fixed immediately after removal in a 10% buffered formalin solution for a maximum of 24 hours at room temperature before being dehydrated and paraffin-embedded under vacuum conditions. Samples were blocked with normal goat serum and incubated with Ki67 (Life Technologies), EGFR (Cell Signaling Technology), and PTEN (Cell Signaling Technology) antibodies. The antigen-antibody reaction was revealed by SignalStain Boost IHC Detection Reagent (8114, Cell Signaling Technology) with 3,3'-diaminobenzidine (DAB) as a substrate (Dako). For IHC on patient samples, tumor tissue was fixed in 10% buffered formalin for 48 hours and embedded in paraffin. Four-micrometer sections were deparaffinized in xylene and hydrated in graded alcohols. For EGFR detection, the antigen was retrieved by protease treatment (8 min at 37°C), and the sections were further incubated at 37°C for 1 hour with a prediluted ready-to-use mouse mAb to EGFR (clone 3C6, Ventana). The antigen-antibody reaction was visualized by ultraView DAB reveal system in a BenchMark XT automated IHC stainer (all from Ventana). For HER3, the antigen retrieval was performed by heating the sections at 97°C for 20 min in EnVision Target Retrieval Solution, High pH (Dako) in PT Link apparatus (Dako). The tissues were then incubated at 37°C for 2 hours with a mouse mAb to HER3 (clone DAK-H3-IC, Dako) diluted 1:50. The antigen-antibody reaction was revealed using EnVision FLEX DAB system in a Dako Autostainer Plus automate. For each patient, the pre- and posttreatment tumor samples were run together. IHC staining was interpreted by an expert pathologist who was blind to patient information. Both EGFR and HER3 abundances were quantified using an arbitrary scale having 0, 0.5, 1, 1.5, 2, 2.5, and 3 as measures of increasing staining intensity. EGFR and HER3 histoscores were defined as a sum of products obtained by multiplying the staining intensity with the percentage of stained cells.

Patient samples

For PDX establishment, fresh tissue was obtained from the Massachusetts General Hospital under Institutional Review Board approval and patient's informed consent. Triple-negative status was determined by the Massachusetts General Hospital Clinical Laboratory and Department of Pathology. Formalin-fixed paraffin-embedded (FFPE) specimens for IHC analyses of EGFR and HER3 abundance were obtained from the institutions participating in two French multicenter pilot phase 2 neoadjuvant trials that tested the efficacy of an anti-EGFR antibody combined to chemotherapy in TNBC stage II to IIIA patients (NCT00933517 and NCT00600249). pCR was the primary endpoint (with clinical response and toxicity as secondary endpoints), for which 47 and 29 patients were evaluated in the panitumumab and cetuximab trials, respectively (table S2). Tumor tissue samples were systematically collected before and at the end of the neoadjuvant treatment at the Jean Perrin

Comprehensive Cancer Center, where molecular and pathological analyses were performed. pCR was evaluated using Chevallier *et al.*'s (34) and Sataloff *et al.*'s (35) classifications.

Fluorescence resonance energy transfer

To monitor FRET between EGFR and HER3, we used fluorescence lifetime imaging microscopy (FLIM), which is a gold standard technique for measuring protein proximity within the typically less than 10-nm range (36–38), and which we pioneered in its application to FFPE cancer samples (39, 40). Two consecutive slices were placed on the same glass slide, and antigen retrieval was performed with the Ventana BenchMark ULTRA system according to the manufacturer's instructions. One slice was stained for EGFR alone [detected by an Alexa Fluor 546-conjugated mAb to EGFR (F4), from the Cancer Research UK (CRUK) repository], and the second slice for EGFR and HER3 [detected by a Cy5-conjugated mAb to HER3 (2F12), Thermo Scientific]. Antibodies were directly labeled according to the manufacturer's protocol with Alexa Fluor 546 and Cy5, respectively. Both antibodies were shown to be specific in either cells overexpressing untagged EGFR (plasmid provided by A. Reynolds, Tumor Angiogenesis Group, The Breakthrough Breast Cancer Research Centre, London) or enhanced green fluorescent protein-tagged HER3 (a gift from S. Roberts, Gray Cancer Institute, Mount Vernon Hospital), or in FFPE sections (fig. S11). Samples were imaged on an “open” microscope automated FLIM system (41). Image analysis was done using newly developed algorithm to create the lifetime filter to eliminate auto-fluorescence, so any lifetime reduction on the masked tumor image will indicate true FRET (42).

Statistical analysis

Two-way *t* tests were performed with GraphPad Prism (GraphPad Software). Error bars represent the SEM, and *P* values are indicated by **P* < 0.05 and ***P* < 0.01. All cellular experiments were repeated at least three times. All the *in vivo* experiments were run with at least seven mice for each treatment arm. Statistical analysis on data related to the French clinical trial samples was performed with Microsoft Excel and Statistics Epidemiology Medicine, a biomedical statistical analysis software created by Kwiatkowski *et al.* (43).

Supplementary Material

Refer to Web version on PubMed Central for supplementary material.

Acknowledgments

We are grateful to C. Abrial and F. Kwiatkowski for statistical support and the Translational Breast Cancer Research Consortium for the TBCRC 001 study.

Funding: The clinical panitumumab study conducted in France was sponsored by Amgen and the Jean Perrin Comprehensive Cancer Center. Preclinical work was funded by Susan G. Komen for the Cure (SAC110046) and the Breast Cancer Research Foundation. King's College London-University College London Comprehensive Cancer Imaging Centre funding was provided by CRUK and the Engineering and Physical Sciences Research Council in association with the Medical Research Council and Department of Health (England; C1519/ A10331) and an FP7-HEALTH-2010 European Union grant entitled “IMAGINT” (grant number 259881). M.E. is an International Sephardic Education Foundation postdoctoral fellow; A.B. holds a Translational Research Fellowship from the Spanish Society of Medical Oncology (SEOM); CM.P. is funded by the National Cancer Institute Breast SPORE (Specialized Program of Research Excellence) program (P50-CA58223-09A1) and the Breast Cancer

Research Foundation; and N. Aceto is a fellow of the Human Frontiers Science Program, the Swiss National Science Foundation, and the Swiss Foundation for Grants in Biology and Medicine.

References and Notes

1. Shah SP, Roth A, Goya R, Oloumi A, Ha G, Zhao Y, Turashvili G, Ding J, Tse K, Haffari G, Bashashati A, Prentice LM, Khattra J, Burleigh A, Yap D, Bernard V, McPherson A, Shumansky K, Crisan A, Giuliany R, Heravi-Moussavi A, Rosner J, Lai D, Birol I, Varhol R, Tam A, Dhalla N, Zeng T, Ma K, Chan SK, Griffith M, Moradian A, Cheng SW, Morin GB, Watson P, Gelmon K, Chia S, Chin SF, Curtis C, Rueda OM, Pharoah PD, Damaraju S, Mackey J, Hoon K, Harkins T, Tadigotla V, Sigaroudinia M, Gascard P, Tlsty T, Costello JF, Meyer IM, Eaves CJ, Wasserman WW, Jones S, Huntsman D, Hirst M, Caldas C, Marra MA, Aparicio S. The clonal and mutational evolution spectrum of primary triple-negative breast cancers. *Nature*. 2012; 486:395–399. [PubMed: 22495314]
2. Foulkes WD, Smith IE, Reis-Filho JS. Triple-negative breast cancer. *N Engl J Med*. 2010; 363:1938–1948. [PubMed: 21067385]
3. Dent R, Hanna WM, Trudeau M, Rawlinson E, Sun P, Narod SA. Pattern of metastatic spread in triple-negative breast cancer. *Breast Cancer Res Treat*. 2009; 115:423–428. [PubMed: 18543098]
4. André F, Zielinski CC. Optimal strategies for the treatment of metastatic triple-negative breast cancer with currently approved agents. *Ann Oncol*. 2012; 23(Suppl. 6):vi46–vi51. [PubMed: 23012302]
5. Carey LA. Directed therapy of subtypes of triple-negative breast cancer. *Oncologist*. 2011; 16(Suppl. 1):71–78. [PubMed: 21278443]
6. Liedtke C, Mazouni C, Hess KR, André F, Tordai A, Mejia JA, Symmans WF, Gonzalez-Angulo AM, Hennessy B, Green M, Cristofanilli M, Hortobagyi GN, Pusztai L. Response to neoadjuvant therapy and long-term survival in patients with triple-negative breast cancer. *J Clin Oncol*. 2008; 26:1275–1281. [PubMed: 18250347]
7. von Minckwitz G, Martin M. Neoadjuvant treatments for triple-negative breast cancer (TNBC). *Ann Oncol*. 2012; 23(Suppl. 6):vi35–vi39. [PubMed: 23012300]
8. Marty B, Maire V, Gravier E, Rigai G, Vincent-Salomon A, Kappler M, Lebigot I, Djelti F, Tourdès A, Gestraud P, Hupé P, Barillot E, Cruzalegui F, Tucker GC, Stern MH, Thiery JP, Hickman JA, Dubois T. Frequent PTEN genomic alterations and activated phosphatidylinositol 3-kinase pathway in basal-like breast cancer cells. *Breast Cancer Res*. 2008; 10:R101. [PubMed: 19055754]
9. Nielsen TO, Hsu FD, Jensen K, Cheang M, Karaca G, Hu Z, Hernandez-Boussard T, Livasy C, Cowan D, Dressler L, Akslen LA, Ragaz J, Gown AM, Gilks CB, van de Rijn M, Perou CM. Immunohistochemical and clinical characterization of the basal-like subtype of invasive breast carcinoma. *Clin Cancer Res*. 2004; 10:5367–5374. [PubMed: 15328174]
10. Carey L, Winer E, Viale G, Cameron D, Gianni L. Triple-negative breast cancer: Disease entity or title of convenience? *Nat Rev Clin Oncol*. 2010; 7:683–692. [PubMed: 20877296]
11. Baselga, J.; Gomez, P.; Awada, A.; Greil, R.; Braga, S.; Climent, M.; Wardley, A.; Zubel, A.; Groos, J.; Kaufmann, B. The addition of cetuximab to cisplatin increases overall response rate (ORR) and progression-free survival (PFS) in metastatic triple-negative breast cancer (TNBC): Results of a randomized phase II study (BALI-1). Paper presented at the 35th Congress of the European Society for Medical Oncology; Milan, Italy. 2010.
12. Carey LA, Rugo HS, Marcom PK, Mayer EL, Esteva FJ, Ma CX, Liu MC, Storniolo AM, Rimawi MF, Forero-Torres A, Wolff AC, Hobday TJ, Ivanova A, Chiu WK, Ferraro M, Burrows E, Bernard PS, Hoadley KA, Perou CM, Winer EP. TBCRC 001: Randomized phase II study of cetuximab in combination with carboplatin in stage IV triple-negative breast cancer. *J Clin Oncol*. 2012; 30:2615–2623. [PubMed: 22665533]
13. Bendell JC, Rodon J, Burris HA, de Jonge M, Verweij J, Birle D, Demanse D, De Buck SS, Ru QC, Peters M, Goldbrunner M, Baselga J. Phase I, dose-escalation study of BKM120, an oral pan-class I PI3K inhibitor, in patients with advanced solid tumors. *J Clin Oncol*. 2012; 30:282–290. [PubMed: 22162589]

14. Chandarlapaty S, Sawai A, Scaltriti M, Rodrik-Outmezguine V, Grbovic-Huezo O, Serra V, Majumder PK, Baselga J, Rosen N. AKT inhibition relieves feedback suppression of receptor tyrosine kinase expression and activity. *Cancer Cell*. 2011; 19:58–71. [PubMed: 21215704]
15. Rodrik-Outmezguine VS, Chandarlapaty S, Pagano NC, Poulikakos PI, Scaltriti M, Moskatel E, Baselga J, Guichard S, Rosen N. mTOR kinase inhibition causes feedback-dependent biphasic regulation of AKT signaling. *Cancer Discov*. 2011; 1:248–259. [PubMed: 22140653]
16. Serra V, Scaltriti M, Prudkin L, Eichhorn PJ, Ibrahim YH, Chandarlapaty S, Markman B, Rodriguez O, Guzman M, Rodriguez S, Gili M, Russillo M, Parra JL, Singh S, Arribas J, Rosen N, Baselga J. PI3K inhibition results in enhanced HER signaling and acquired ERK dependency in HER2-overexpressing breast cancer. *Oncogene*. 2011; 30:2547–2557. [PubMed: 21278786]
17. Sergina NV, Rausch M, Wang D, Blair J, Hann B, Shokat KM, Moasser MM. Escape from HER-family tyrosine kinase inhibitor therapy by the kinase-inactive HER3. *Nature*. 2007; 445:437–441. [PubMed: 17206155]
18. Wheeler DL, Huang S, Kruser TJ, Nechrebecki MM, Armstrong EA, Benavente S, Gondi V, Hsu KT, Harari PM. Mechanisms of acquired resistance to cetuximab: Role of HER (ErbB) family members. *Oncogene*. 2008; 27:3944–3956. [PubMed: 18297114]
19. Morrison MM, Hutchinson K, Williams MM, Stanford JC, Balko JM, Young C, Kuba MG, Sánchez V, Williams AJ, Hicks DJ, Arteaga CL, Prat A, Perou CM, Earp HS, Massarweh S, Cook RS. ErbB3 downregulation enhances luminal breast tumor response to antiestrogens. *J Clin Invest*. 2013; 123:4329–4343. [PubMed: 23999432]
20. Kirouac DC, Du JY, Lahdenranta J, Overland R, Yarar D, Paragas V, Pace E, McDonagh CF, Nielsen UB, Onsum MD. Computational modeling of ERBB2-amplified breast cancer identifies combined ErbB2/3 blockade as superior to the combination of MEK and AKT inhibitors. *Sci Signal*. 2013; 6:ra68. [PubMed: 23943608]
21. Okuzumi T, Fiedler D, Zhang C, Gray DC, Aizenstein B, Hoffman R, Shokat KM. Inhibitor hijacking of Akt activation. *Nat Chem Biol*. 2009; 5:484–493. [PubMed: 19465931]
22. Folkes AJ, Ahmadi K, Alderton WK, Alix S, Baker SJ, Box G, Chuckowree IS, Clarke PA, Depledge P, Eccles SA, Friedman LS, Hayes A, Hancox TC, Kugendradas A, Lensun L, Moore P, Olivero AG, Pang J, Patel S, Pergl-Wilson GH, Raynaud FI, Robson A, Saghir N, Salphati L, Sohal S, Ultsch MH, Valenti M, Wallweber HJ, Wan NC, Wiesmann C, Workman P, Zhyvoloup A, Zvelebil MJ, Shuttleworth SJ. The identification of 2-(1*H*-indazol-4-yl)-6-(4-methanesulfonyl-piperazin-1-ylmethyl)-4-morpholin-4-yl-thieno[3,2-*d*]pyrimidine (GDC-0941) as a potent, selective, orally bioavailable inhibitor of class I PI3 kinase for the treatment of cancer. *J Med Chem*. 2008; 51:5522–5532. [PubMed: 18754654]
23. Schaefer G, Haber L, Crocker LM, Shia S, Shao L, Dowbenko D, Totpal K, Wong A, Lee CV, Stawicki S, Clark R, Fields C, Lewis Phillips GD, Prell RA, Danilenko DM, Franke Y, Stephan JP, Hwang J, Wu Y, Bostrom J, Sliwkowski MX, Fuh G, Eigenbrot C. A two-in-one antibody against HER3 and EGFR has superior inhibitory activity compared with monospecific antibodies. *Cancer Cell*. 2011; 20:472–486. [PubMed: 22014573]
24. Krumbach R, Schüler J, Hofmann M, Giesemann T, Fiebig HH, Beckers T. Primary resistance to cetuximab in a panel of patient-derived tumour xenograft models: Activation of MET as one mechanism for drug resistance. *Eur J Cancer*. 2011; 47:1231–1243. [PubMed: 21273060]
25. Garrett JT, Olivares MG, Rinehart C, Granja-Ingram ND, Sánchez V, Chakrabarty A, Dave B, Cook RS, Pao W, McKinley E, Manning HC, Chang J, Arteaga CL. Transcriptional and posttranslational up-regulation of HER3 (ErbB3) compensates for inhibition of the HER2 tyrosine kinase. *Proc Natl Acad Sci U S A*. 2011; 108:5021–5026. [PubMed: 21385943]
26. Yan Y, Serra V, Prudkin L, Scaltriti M, Murli S, Rodríguez O, Guzman M, Sampath D, Nannini M, Xiao Y, Wagle MC, Wu J, Hampton GM, Wongchenko M, Ramakrishnan V, Lackner MR, Saura C, Roda D, Cervantes A, Tabernero J, Patel P, Baselga J. Evaluation and clinical analyses of downstream targets of the Akt inhibitor GDC-0068. *Clin Cancer Res*. 2013; 19:6976–6986. [PubMed: 24141624]
27. García-García C, Ibrahim YH, Serra V, Calvo MT, Guzmán M, Grueso J, Aura C, Pérez J, Jessen K, Liu Y, Rommel C, Tabernero J, Baselga J, Scaltriti M. Dual mTORC1/2 and HER2 blockade results in antitumor activity in preclinical models of breast cancer resistant to anti-HER2 therapy. *Clin Cancer Res*. 2012; 18:2603–2612. [PubMed: 22407832]

28. Holland JP, Sheh Y, Lewis JS. Standardized methods for the production of high specific-activity zirconium-89. *Nucl Med Biol.* 2009; 36:729–739. [PubMed: 19720285]
29. Viola-Villegas NT, Rice SL, Carlin S, Wu X, Evans MJ, Sevak KK, Drobjnak M, Ragupathi G, Sawada R, Scholz WW, Livingston PO, Lewis JS. Applying PET to broaden the diagnostic utility of the clinically validated CA19.9 serum biomarker for oncology. *J Nucl Med.* 2013; 54:1876–1882. [PubMed: 24029655]
30. Elkabets M, Vora S, Juric D, Morse N, Mino-Kenudson M, Muranen T, Tao J, Campos AB, Rodon J, Ibrahim YH, Serra V, Rodrik-Outmezguine V, Hazra S, Singh S, Kim P, Quadt C, Liu M, Huang A, Rosen N, Engelman JA, Scaltriti M, Baselga J. mTORC1 inhibition is required for sensitivity to PI3K p110a inhibitors in PIK3CA-mutant breast cancer. *Sci Transl Med.* 2013; 5:196ra199.
31. Kim P, Liu X, Lee T, Liu L, Barham R, Kirkland R, Leesman G, Kuller A, Ybarrondo B, Ng SC, Singh S. Highly sensitive proximity mediated immunoassay reveals HER2 status conversion in the circulating tumor cells of metastatic breast cancer patients. *Proteome Sci.* 2011; 9:75. [PubMed: 22172159]
32. Stott SL, Hsu CH, Tsukrov DI, Yu M, Miyamoto DT, Waltman BA, Rothenberg SM, Shah AM, Smas ME, Korir GK, Floyd FP, Gilman AJ, Lord JB, Winokur D, Springer S, Irimia D, Nagrath S, Sequist LV, Lee RJ, Isselbacher KJ, Maheswaran S, Haber DA, Toner M. Isolation of circulating tumor cells using a microvortex-generating herringbone-chip. *Proc Natl Acad Sci U S A.* 2010; 107:18392–18397. [PubMed: 20930119]
33. Yu M, Bardia A, Wittner BS, Stott SL, Smas ME, Ting DT, Isakoff SJ, Ciciliano JC, Wells MN, Shah AM, Concannon KF, Donaldson MC, Sequist LV, Brachtel E, Sgroi D, Baselga J, Ramaswamy S, Toner M, Haber DA, Maheswaran S. Circulating breast tumor cells exhibit dynamic changes in epithelial and mesenchymal composition. *Science.* 2013; 339:580–584. [PubMed: 23372014]
34. Chevallier B, Roche H, Olivier JP, Chollet P, Hurlteloup P. Inflammatory breast cancer. Pilot study of intensive induction chemotherapy (FEC-HD) results in a high histologic response rate. *Am J Clin Oncol.* 1993; 16:223–228. [PubMed: 8338056]
35. Sataloff DM, Mason BA, Prestipino AJ, Seinige UL, Leber CP, Baloch Z. Pathologic response to induction chemotherapy in locally advanced carcinoma of the breast: A determinant of outcome. *J Am Coll Surg.* 1995; 180:297–306. [PubMed: 7874340]
36. Bublil EM, Pines G, Patel G, Fruhwirth G, Ng T, Yarden Y. Kinase-mediated quasi-dimers of EGFR. *FASEB J.* 2010; 24:4744–4755. [PubMed: 20682838]
37. Morris JR, Boutell C, Keppler M, Densham R, Weekes D, Alamshah A, Butler L, Galanty Y, Pagon L, Kiuchi T, Ng T, Solomon E. The SUMO modification pathway is involved in the BRCA1 response to genotoxic stress. *Nature.* 2009; 462:886–890. [PubMed: 20016594]
38. Legg JW, Lewis CA, Parsons M, Ng T, Isacke CM. A novel PKC-regulated mechanism controls CD44-ezrin association and directional cell motility. *Nat Cell Biol.* 2002; 4:399–407. [PubMed: 12032545]
39. Ng T, Squire A, Hansra G, Bornancin F, Prevostel C, Hanby A, Harris W, Barnes D, Schmidt S, Mellor H, Bastiaens PIH, Parker PJ. Imaging protein kinase Ca activation in cells. *Science.* 1999; 283:2085–2089. [PubMed: 10092232]
40. Parsons M, Ng T. Intracellular coupling of adhesion receptors: Molecular proximity measurements. *Methods Cell Biol.* 2002; 69:261–278. [PubMed: 12070997]
41. Barber PR, Tullis ID, Pierce GP, Newman RG, Prentice J, Rowley MI, Matthews DR, Ameer-Beg SM, Vojnovic B. The Gray Institute ‘open’ high-content, fluorescence lifetime microscopes. *J Microsc.* 2013; 251:154–167. [PubMed: 23772985]
42. Barber PR, Tullis ID, Rowley MI, Martins CD, Weitsman G, Lawler K, Coffey M, Woodman N, Gillett CE, Ng T, Vojnovic B. The Gray Institute Open Microscopes applied to radiobiology and protein interaction studies. *Proc SPIE.* in press.
43. Kwiatkowski F, Girard M, Hacene K, Berlie J. Sem: A suitable statistical software adapted for research in oncology. *Bull Cancer.* 2000; 87:715–721. [PubMed: 11084535]

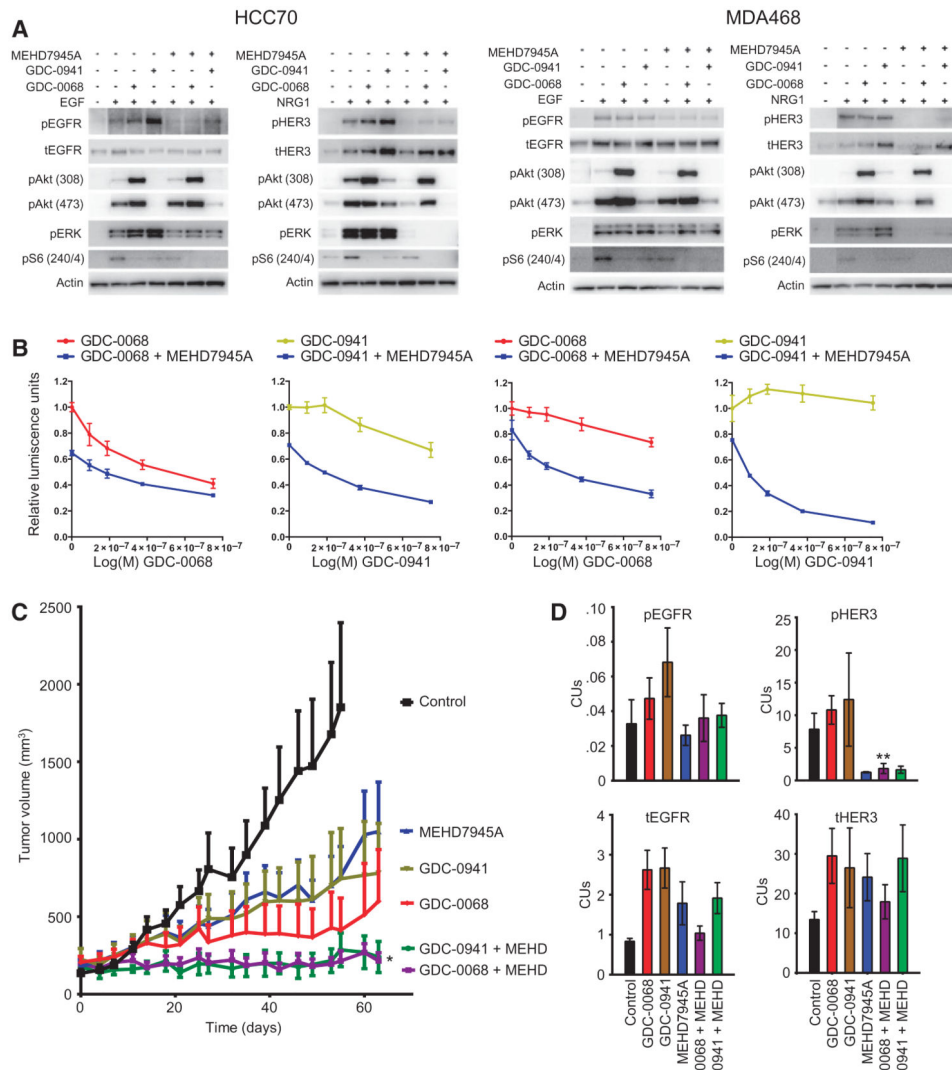


Fig. 1. Therapeutic activity of combined inhibition of EGFR, HER3, and the PI3K-Akt pathway in TNBC preclinical models

(A) Western blot for total and phosphorylated EGFR, HER3, and downstream proteins HCC70 and MDA-MB-468 (MDA468) cells after the indicated treatments for 24 hours: EGF or NRG1, 4 ng/ml; MEHD7945A, 10 nM; GDC-0068 and GDC-0941, 1 μ M. (B) Analysis of the proliferation of HCC70 (left) and MDA-MB-468 cells (right) treated for 5 days as indicated; concentrations as in (A). (C) Tumor growth curves of TNBC PDX treated as indicated: MEHD7945A (MEHD), 10 mg/kg twice weekly; GDC-0941, 75 mg/kg daily; GDC-0068, 40 mg/kg daily. (D) CEER analysis of total and phosphorylated EGFR and HER3 in PDXs treated as indicated. Blots in (A) are representative of and data in (B) are means \pm SEM from two experiments. $n = 8$ and $n = 3$ for each treatment arms in (B) and (D), respectively; $*P = 0.048$ in (C), GDC-0941 + MEHD versus GDC-0941, and $*P = 0.007$, GDC-0068 + MEHD versus GDC-0068. (D) $**P = 0.054$, GDC-0941 + MEHD versus GDC-0941, two-sided Student's *t* test.

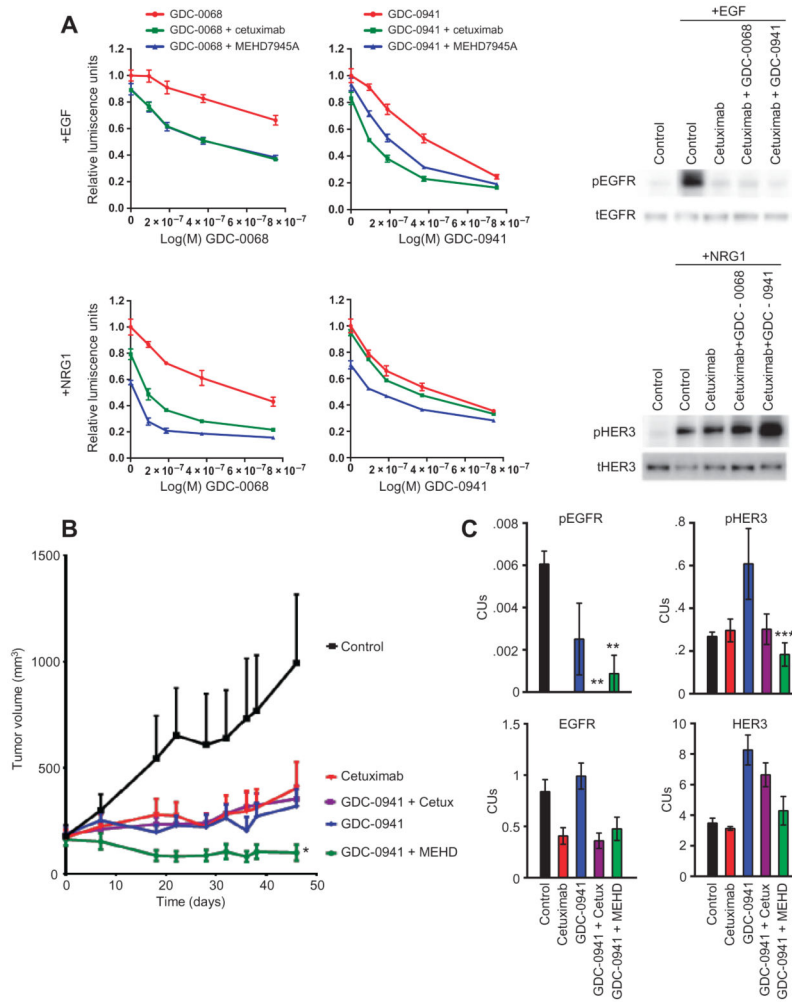


Fig. 2. Efficacy of MEHD7945A or cetuximab in combination with PI3K inhibition
(A) Left: Proliferation analysis of HCC70 cells treated for 5 days as indicated in the presence of EGF (top) or NRG1 (bottom). MEHD7945A (MEHD) and cetuximab (Cetux), 10 nM; GDC-0068 and GDC-0941, 1 μ M. Right: Western blot for phosphorylated and total EGFR and HER3 in HCC70 cells treated as indicated. Blots are representative of two experiments. **(B)** Tumor growth curves of HCC70 xenografts treated as indicated, doses as in Fig. 1A. **(C)** CEER analysis of active and total EGFR and HER3 in HCC70 xenografts treated as indicated. Data are means \pm SEM. $n = 8$ and $n = 3$ for each treatment arms in **(B)** and **(D)**, respectively, at least three tumors per condition; **(B)** $*P = 0.020$, GDC-0941 + MEHD versus GDC-0941, and $P = 0.0054$, GDC-0941 + MEHD versus GDC-0941 + Cetux. **(C)** $**P = 0.0004$, GDC-0941 + MEHD versus control, and $P < 0.0001$, GDC-0941 + Cetux versus control. **(C)** $***P = 0.054$, GDC-0941 + MEHD versus GDC-0941, Student's t test.

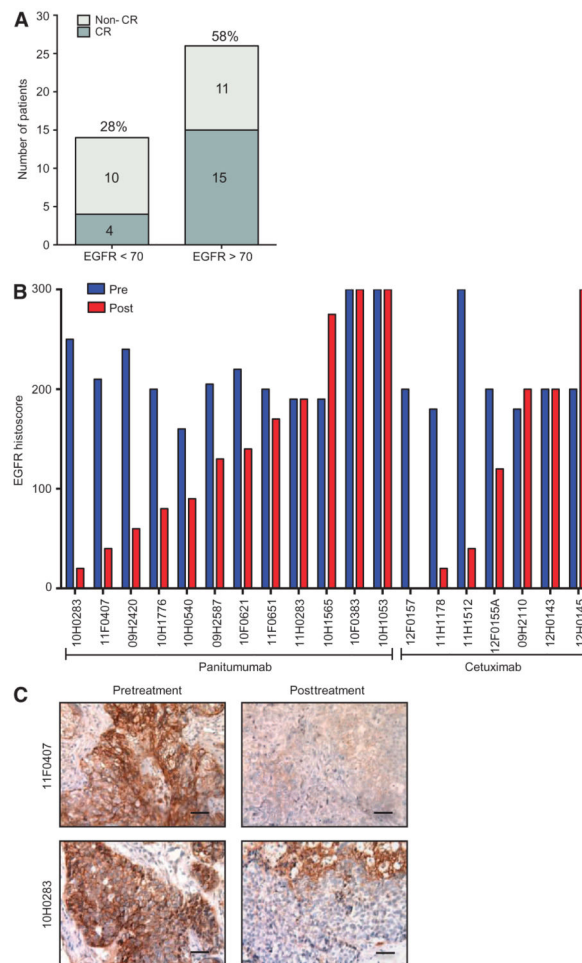


Fig. 3. EGFR expression and response to anti-EGFR therapy in TNBC patients

(A) Correlation between the abundance of EGFR (table S2) and pCR in 47 TNBC patients treated with panitumumab combination therapy (receiver operating characteristic curve, $P = 0.08$). (B) EGFR abundance in tumors before and after treatment with either panitumumab or cetuximab combination therapy in patients who did not achieve pCR ($P = 0.0048$). (C) Representative IHC images ($\times 25$ magnification) of EGFR abundance in residual tumors (posttreatment) versus baseline specimens (pre-treatment). Scale bars, 80 μm .

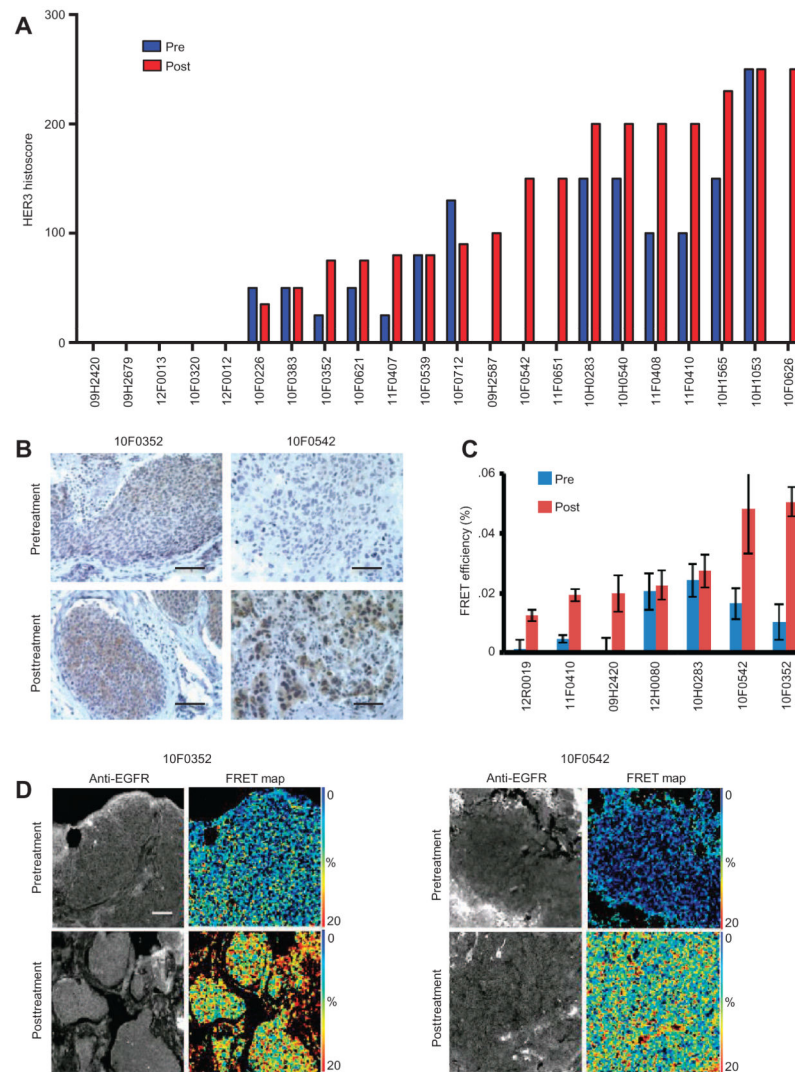


Fig. 4. HER3 expression and response to anti-EGFR therapy in TNBC patients
(A) HER3 abundance by IHC in tumors before and after panitumumab-based treatment in patients who did not achieve pCR ($P = 0.0028$). **(B)** Representative IHC ($\times 25$ magnification) from two patient tumors analyzed in **(A)**. Scale bars, 80 μm . **(C)** FRET analysis of HER3-EGFR dimerization in residual tumors from a subset of patients who did not achieve pCR after treatment with panitumumab/cetuximab-based therapy. **(D)** Representative time-resolved immunofluorescence images ($\times 20$ magnification) from two tumors analyzed in **(A)** to **(C)**. Grayscale image shows intensity of the donor fluorophore, and pseudocolor image shows the pixel-by-pixel FRET efficiency values. Scale bar, 50 μm .